(15) is expressed as follows.

$$\begin{aligned}\boldsymbol{R}(n) &= \mathrm{E}\left[\boldsymbol{y}(n)\boldsymbol{y}^T(n)\right] \\ &= \sum_{k=1}^{N_u} \boldsymbol{G}_k(n)\boldsymbol{G}_k^T(n) + \sigma_n^2 \boldsymbol{I}_L, \end{aligned} \tag{21}$$

where, $\mathrm{E}[\cdot]$ and $\boldsymbol{I}_L$ denote the mathematical expectation and a L-by-L identity matrix. Based on the MMSE criterion, the optimum filter weight for MMSE combining case converges into the following solution.

$$\begin{aligned}\boldsymbol{w}_{\mathrm{MMSE}}(n) &= \arg\min_{\boldsymbol{w}} \mathrm{E}\left[\left(\boldsymbol{w}^T(n)\boldsymbol{y}_l(n) - d_n^1\right)^2\right] \\ &= \boldsymbol{R}^{-1}(n)\boldsymbol{p}(n), \end{aligned} \tag{22}$$

where $\boldsymbol{p}(n)$ is given by

$$\begin{aligned}\boldsymbol{p}(n) &= \mathrm{E}\left[\boldsymbol{y}(n)d_1(n)\right] \\ &= \boldsymbol{g}_{1,N_l}(n). \end{aligned} \tag{23}$$

When short code spreading is employed (i.e., $J = 1$), the correlation matrix and the steering vector do not depend on n, i.e., $\boldsymbol{R}(n) = \boldsymbol{R}$, $\boldsymbol{p}(n) = \boldsymbol{p}$. Accordingly, the combining weight is uniqely determined as $\boldsymbol{w}_{\mathrm{MMSE}}(n) = \boldsymbol{w}_{\mathrm{MMSE}}$. However, in the case of CH ($J \geq 2$), since J kinds of sequences are used, the calculation of $\boldsymbol{R}(j)$ and $\boldsymbol{w}(j)$ for $0 \leq j < J$ must be effectuated. In the case of MRC combining receiver, the weight is simply obtained as

$$\boldsymbol{w}_{\mathrm{MRC}}(n) = \boldsymbol{\lambda}, \tag{24}$$

where $\boldsymbol{\lambda} = [\lambda_1, \ldots, \lambda_L]^T$.

3.2. Derivation of Signal-to-Interface Plus Noise Ratio

Signal-to-interference plus noise ratio (SINR) is derived in order to obtain the BER expression. In this paper, in order to simplify the analysis, MUI and ISI are both assumed to be Gaussian distribution (Gaussian approximation). By using the weight derived in the (22) and (24), the SINR per symbol at the output of the RAKE receiver for both MRC and MMSE combining can easily written as

$$\gamma_n = \frac{\boldsymbol{w}^T(n)\boldsymbol{R}_s(n)\boldsymbol{w}(n)}{\boldsymbol{w}^T(n)\boldsymbol{R}_I(n)\boldsymbol{w}(n)}, \tag{25}$$

where $\boldsymbol{R}_s$ and $\boldsymbol{R}_I$ denote the correlation matrix for the desired output and for the total interference including ISI, MUI, and AWGN, given by

$$\boldsymbol{R}_s(n) = \boldsymbol{g}_{1,N_l}(n)\boldsymbol{g}_{1,N_l}^T(n) \tag{26}$$

$$\boldsymbol{R}_I(n) = \boldsymbol{R}(n) - \boldsymbol{R}_s(n). \tag{27}$$

When using multiple spreading sequence, each SINR is averaged as

$$\bar{\gamma} = \frac{1}{J}\sum_{j=0}^{J-1}\gamma_j. \tag{28}$$

3.3. Upper Bound of Bit Error Rate

The upper bound of the BER of any convolutional codes can be obtained from the generating function $T(X, Y)$. The union bound of the BER is given by [12]

$$P_b < \frac{1}{k}\frac{dT(X,Y)}{dY}\Big|_{Y=1} \tag{29}$$

$$= \frac{1}{k}\sum_{d=d_f}^{\infty} B_d X^d, \tag{30}$$

where $X = \exp(-\bar{\gamma})$. Here the SINR derived in (25) is a function of α_l^k and τ_l^k for $1 \leq k \leq N_u$, $1 \leq l \leq L$. Because SV model is not a stochastic model, it is difficult to obtain an exact solution of average bit error probability. Thus, it is numerically calculated.

4. Numerical Results

In this section, the bit error performance of SO coded scheme is compared with the other convolutional coded scheme based on computer simulations.

4.1. Simulation Parameters

Table 1 shows the parameters applied for convolutional codes (CC) and spreading sequences. As shown in this table, three types of convolutional codes, that is, CC of coding rate $1/2$ (denoted as CC 1 in Table 1) and CC of coding rate $1/4$ (denoted as CC 2 in Table 1), as well as SOCC, are considered. For each code, two different constraint lengths, $K = 5$ and 6, are considered. Note that for SOCC, coding rate is given by $1/8$ and $1/16$ for $K = 5$ and 6, respectively, from the relationship between the constraint length and the coding rate. In order to make a fair comparison, all codes have the same number of states in trellis diagram (or equivalently, the same memory size at the encoder). At the decoder, soft-decision Viterbi decoding is assumed for each scheme. As for the spreading sequence, Gold sequences of length N_c are employed. The length of Gold sequences are set so that the total bandwidth expansion factor $N = N_c/R_c$ is almost the same ($N \simeq 255$ in this case) for all schemes. The number of RAKE fingers is fixed to $L = 8$ for all schemes. The pulse duration and the chip duration are both 2.0 ns. The data transmission rate is given by $R_b = 1/(NT_c)$. Because of the size limitation, only the result for channel model (CM) 3 is shown. Since CM 3 has relatively large number of paths and delay-spread, the performance degradation due to ISI and MUI can be easily observed. Although $L = 8$ is employed in this paper, the bigger the values given to L are, the more significant the performance improvement becomes. This is the trade-off between performance improvement and implementation complexity.

Table 1. Coding and spreading parameters

Scheme	Constraint length (K)	Coding rate (R_c)	Generating function	Sequence length (N_c)	Total spreading factor (N)
CC1	5	1/2	$[23, 35]_8$	127	254
	6	1/2	$[53, 75]_8$	127	254
CC2	5	1/4	$[25, 27, 33, 37]_8$	63	252
	6	1/4	$[53, 67, 71, 75]_8$	63	252
SOCC	5	1/8	–	31	248
	6	1/16	–	15	240
Uncoded	–	1	–	255	255

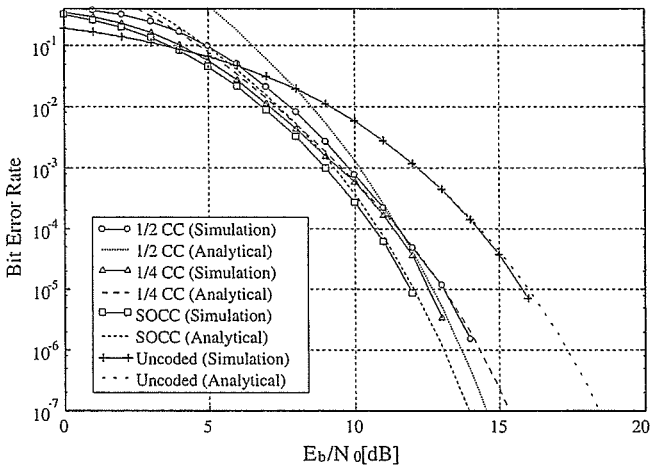

Figure 4. Comparison of BER for different convolutional coding schemes in terms of E_b/N_0 for MRC-RAKE receiver for $L = 8$, $N_u = 1$, $K = 5$, Channel Model=CM3.

4.2. Performance for Single-User ISI Channel

Figure 4 shows the BER versus SNR per information bit, E_b/N_0 , where E_b is the average received energy per information bit. The solid lines and the dotted lines represent the Monte–Carlo simulation results and the analytical upper bound of BER for MRC-RAKE receiver. In the Monte-Carlo simulation, 30, 000 bits are sent for each channel and BERs are averaged over 100 different multipath channels. In this figure, simulation results and analytical results are in good agreement for all schemes. In a single-user environment, the receiver suffers only from ISI. This figure shows that performance of SOCC does not deteriorate so much because of its strong error correction capability (or large free distance), though the performance depends on the total bandwidth expansion factor. Therefore, in this case, MMSE receiver is not necessary.

4.3. Performance for Multi-User Channel

Figures 5–8 show the BER versus E_b/N_0 for multipath and multiple access environment. Again, channel model is CM 3, and the number of users is 30. For simplicity, we assume that the received energies of all users are the same; i.e., $A_k = 1$ for all k. In our simulations, we

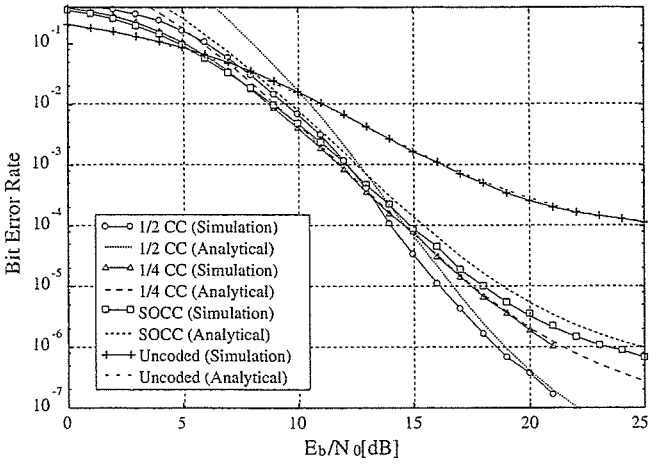

Figure 5. Comparison of BER for different convolutional coding schemes in terms of E_b/N_0 for MRC-RAKE receiver for $L = 8$, $N_u = 30$, $K = 5$, $J = 1$, Channel Model=CM3.

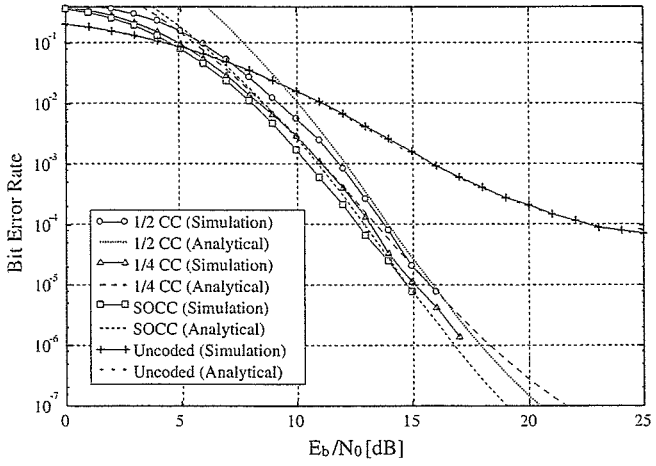

Figure 6. Comparison of BER for different convolutional coding schemes in terms of E_b/N_0 for MRC-RAKE receiver for $L = 8$, $N_u = 30$, $K = 5$, $J = 4$, Channel Model=CM3.

generate 100 channel impulse responses for the desired user in the same way as in the previous case. An additional assumptions are made that all users experience independent, but the same type of fading, that is, all users experience CM 3.

Figure 5 shows the performance of MRC-RAKE receiver using single spreading sequence ($J = 1$). This figure shows that the performance deteriorates gradually when the coding rate decreases (except the uncoded case). The reason for the performance degradation is that, in the system employing single spreading, the performance largely depends on the length of the spreading sequence because the interference coefficient remains unchanged during the transmission time. As a result, the variance of the interference terms increase.

Figure 6 shows the BER performance of MRC-RAKE receiver using CH scheme with $J = 4$. As opposed to the previous result, in Figure 6, the BER performance is improved as the coding rate decreases. This is due to the fact that by using multiple spreading sequence, the

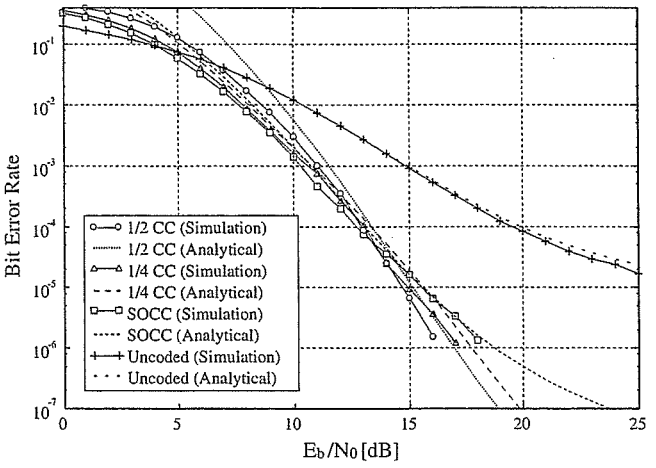

Figure 7. Comparison of BER for different convolutional coding schemes in terms of E_b/N_0 for MMSE-RAKE receiver for $L = 8$, $N_u = 30$, $K = 5$, $J = 1$, Channel Model=CM3.

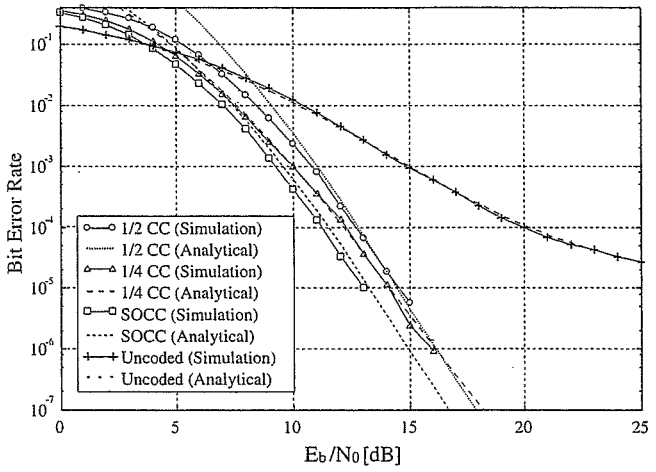

Figure 8. Comparison of BER for different convolutional coding schemes in terms of E_b/N_0 for MMSE-RAKE receiver for $L = 8$, $N_u = 30$, $K = 5$, $J = 4$, Channel Model=CM3.

interference coefficients change from symbol to symbol, which allows the interference terms to be treated as noise. In other words, MUI is closer to Gaussian distribution than that when single spreading sequence is employed.

Next, Figures 7 and 8 show the BER performance of MMSE-RAKE combining receiver for $J = 1$ (single spreading sequence) and $J = 4$ (CH). In contrast to the MRC combining scheme, in Figure 7, the BER performance does not deteriorate even in the case of $J = 1$, because the MMSE filter effectively suppresses the interference. Figures 9 and 10 show the theoretical upper bound of BER in terms of the active number of users. From these figures, we can find that the lower the coding rate is, the better the performance becomes. Moreover, the difference is bigger in Figure 9 than Figure 10. The performance of $1/2$ CC is not improved even if MMSE receiver is employed.

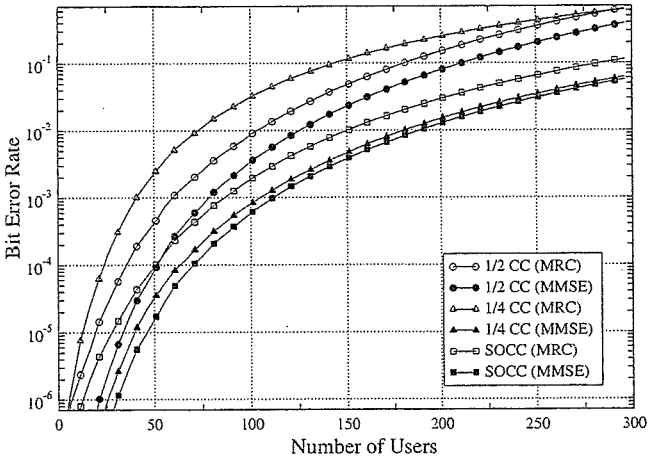

Figure 9. Comparison of BER for different convolutional coding schemes in terms of number of active users for both MRC-RAKE receiver and MMSE-RAKE receiver for $E_b/N_0 = 15$ [dB], $K = 5$, $L = 8$, Channel Model=CM3.

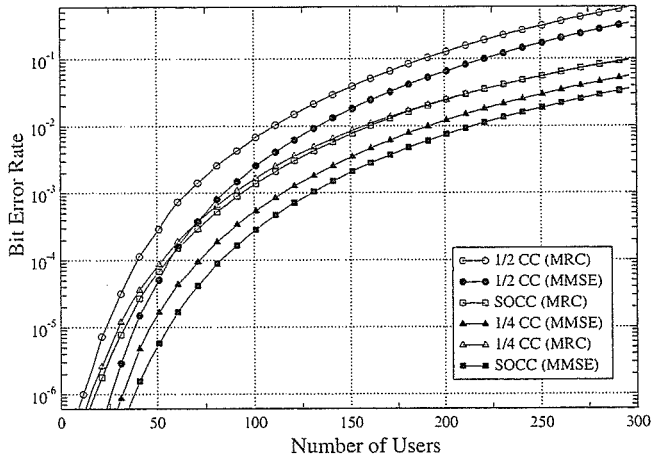

Figure 10. Comparison of BER for different convolutional coding schemes in terms of number of active users for both MRC-RAKE receiver and MMSE-RAKE receiver for $E_b/N_0 = 15$ [dB], $K = 6$, $L = 8$, Channel Model=CM3.

4.4. SPECTRAL EFFICIENCY

Finally, Figures 11 and 12 show the comparison of the achievable spectral efficiency in terms of the total spreading factor. Here the spectral efficiency is defined as $N_u R_b$, where N_u denotes the maximum number of users to achieve a certain performance. A target BER, $P_b < 10^{-4}$, is assumed. It can be found that the lower the coding rate is, the bigger the achievable system capacity becomes. In addition to this, MMSE receiver effectively suppresses the interference from other users and further increases the system capacity.

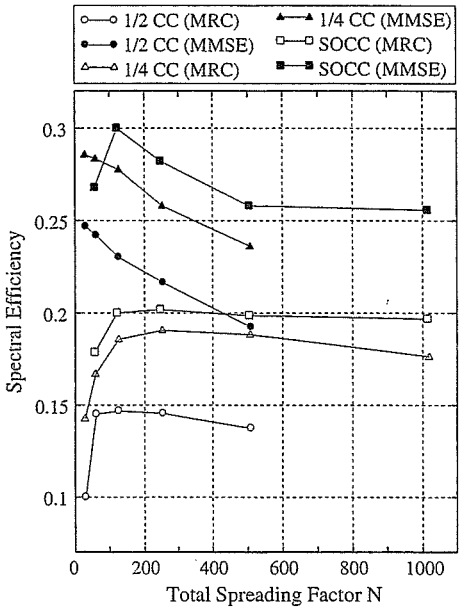

Figure 11. Achievable spectral efficiency in terms of total spreading factor for $E_b/N_0 = 15$[dB], BER=10^{-4}, $L = 8$, $J = 4$, $K = 5$, Channel Model=CM3.

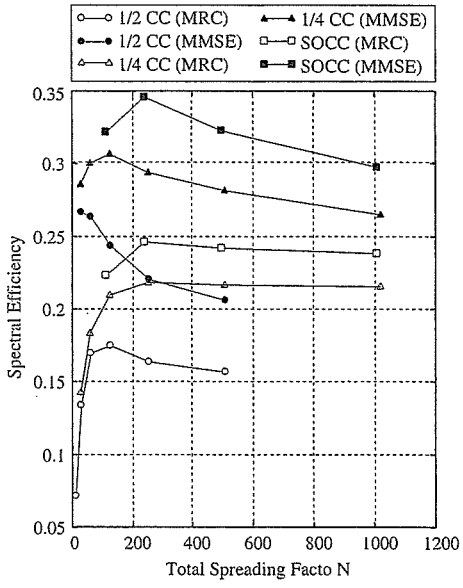

Figure 12. Achievable spectral efficiency in terms of total spreading factor for $E_b/N_0 = 15$[dB], BER=10^{-4}, $L = 8$, $J = 4$, $K = 6$, Channel Model=CM3.

5. Conclusions

In this paper, the use of SOCC to improve the average BER performance of DS-UWB systems over multipath and multiple access environment was studied. Analysis of the effect of MUI and ISI on the BER performance of SOCC assuming two types of receiver, MRC-RAKE

receiver and MMSE-RAKE receiver, was performed. Our analysis showed that in the case of employing simple MRC-RAKE receiver, the BER performance of SOCC was affected by MUI and ISI because of the short length of spreading sequence.

In order to combat MUI and ISI, first CH scheme was employed in conjunction with SOCC to make the interference independent from symbol to symbol. The results showed that SO coded scheme outperforms the higher-rate conventional convolutional coded scheme for multipath and multiple access channels when it is combined with CH. Analysis of MMSE-RAKE receiver to suppress interferences, was also performed. The BER performance of SOCC using MMSE-RAKE receiver was better than the one of higher-rate codes even if short-spreading codes were used. In the case of MMSE receiver, the use of CH improved the BER performance.

A conclusion that can be drawn is that, for UWB systems, low-rate channel code is effective if it is combined with CH or some interference suppression strategy like MMSE filtering. Also, it can be concluded that for low-data rate and low-cost applications, such as low-rate WPAN, combined low-rate coding and scrambling, or CH is suitable. For high-rate WPAN using relatively large number of RAKE fingers, combined SOCC and MMSE-RAKE receiver is effectively increase the system capacity.

References

1. A. J. Viterbi, *CDMA : Principles of Spread Spectrum Communication*. Addison Wesley, 1995.
2. A. J. Viterbi, "Very Low Rate Convolution Codes for Maximum Theoretical Performance of Spread-Spectrum Multiple-Access Channels," *IEEE Journal on Selected Areas in Commun.*, Vol. 8, No. 4, pp. 641–649, 1990.
3. P. D. Shaft, "Low-Rate Convolutional Code Applications in Spread-Spectrum communications," *IEEE Transactions on Communications*, Vol. 25, No. 8, pp. 815–822, 1977.
4. P. Frenger, P. Orten, and T. Ottosson, "Code-Spread CDMA Using Maximum Free Distance Low-Rate Convolutional Codes," *IEEE Transactons on Communication*, Vol. 48, No. 1, pp. 135–144, 2000.
5. M. L. Welborn, "System Considerations for Ultra-Wideband Wireless Networks," *Proceedings of the IEEE Radio and Wireless Conf.*, Boston, MA, Aug. 19–22, 2001.
6. A. R. Fourouzan, M. Nasiri-Kenari, and J. A. Salehi, "Performance Analysis of Time-Hopping Spread-Spectrum Multiple-Access Systems: Uncoded and Coded Schemes", *IEEE Trasactions on Communications*, Vol.1, No. 4, pp. 671–681, 2002.
7. A. R. Fourouzan, M. Nasiri-Kenari, and J. A. Salehi, "Low-Rate Convolutionally Encoded Time-Hopping Spread Spectrum Multiple Access Systems", *Proceedings of the IEEE International Symposium on Personal, Indoor and Mobile Radio Communications*, Barcelona, Spain vol. 2, pp. 1555–1558, 2000.
8. J. Foerster, Channel Modeling Sub-committee Report Final, IEEE P802.15 Working Group for Wireless Personal Area Networks (WPANs), IEEE p802.15 02/49orl SG3a, Feb 2002.
9. N. Yamamoto, "Performance Evaluation of internally Low Rate Turbo Coded UWB-IR Systems", *IEICE technical report*, Microwaves, pp. 135–140, 2003.
10. K. Tang, P. H. Siegel, and L. B. Milstein, "A Comparison of Long versus Short Spreading Sequences in Coded Asynchronous DS-CDMA Systems," *IEEE Journal on Selected Areas in Communication*, Vol. 19, pp. 1614–1624, 2001.
11. J. D. Choi, "Performance of Ultra-Wideband Communications With Suboptimal Receivers in Multipath Channels," *IEEE Journal of Selected Areas Communication*, Vol. 20, No. 9, pp. 1754–1766, 2002.
12. J. G. Proakis, *Digital Communications*. Mcgraw-Hill, 1995.

Tomoko Matsumoto was born in Ehime, Japan, in 1981. She received the M.S. degree in Division of Physics, Electrical and Computer Engineering from Yokohama National University, Yokohama, Japan, in 2005. She is currently working toward the Ph.D. degree in electrical and computer engineering at Yokohama National University, Yokohama, Japan. Her research interests include ultra-wideband communications, channel coding in wireless communications and information theory. She is a student member of the IEICE and IEEE.

Ryuji Kohno received the Ph.D. degree from the University of Tokyo in 1984. Dr. Kohno is currently a Professor of the Division of Physics, Electrical, and Computer Engineering, Yokohama National University. In his career, he was a director of Advanced Telecommunications Laboratory of SONY CSL during 1998–2002 and currently a director of UWB Technology institute of National Institute of Information and Communications Technology (NICT). In his academic activities, he was elected as a member of the Board of Governors of IEEE Information Theory (IT) Society in 2000 and 2003. He has played a role of an editor of the IEEE Transactions on IT, Communications, and Intelligent Transport Systems (ITS). He is a fellow of IEICE, vice-president of Engineering Sciences Society of IEICE and has been the Chairman of the IEICE Technical Committee on Spread Spectrum Technology, that on ITS, and that on Software Defined Radio (SDR). Prof. Kohno has contributed for organizing many international conferences, such as an chair-in honor of 2002 & 2003 International Conference of SDR (SDR'02 & SDR'03), a TPC co-chair of 2003 International Workshop on UWB Systems(IWUWBS'03), and a general co-chair of 2003 IEEE International Symposium on IT (ISIT'03), that of Joint UWBST&IWUWB'04 and IWUWBT'05, and so on. He was awarded IEICE Greatest Contribution Award and NTT DoCoMo Mobile Science Award in 1999 and 2002, respectively.

IEICE TRANS. FUNDAMENTALS, VOL.E89–A, NO.11 NOVEMBER 2006

PAPER Special Section on Wide Band Systems

Interference Reduction Using a Novel Pulse Set for UWB-CDMA Systems

Hiroki HARADA[†a)], *Student Member and* Ryuji KOHNO[†b)], *Fellow*

SUMMARY A novel UWB system for a new indoor short distance radio-communication is examined. Various types of UWB systems have been proposed in the literature. Particularly direct sequence (DS) systems and time hopping (TH) systems are attractive due to low power consumption and a simple transceiver construction. In this paper, we consider to apply *modulated and modified Hermite pulses* (MMHP) for both DS-UWB and TH-UWB systems. Furthermore, MMHP are extended to a novel pulse set referred as *limited bandwidth MMHP set* in order to reduce various interferences. It is composed of pseudo-orthogonal pulses that have both good auto-correlation characteristics in all orders and low cross-correlation characteristics between different orders. The proposed pulse set also have some specific notches, which can be used to reduce narrow-band interference (NBI). Additionally, we propose a novel pulse shape hopping that employs the proposed MMHP set. Multi-user interference (MUI) and inter-symbol interference (ISI) can be reduced by such a pulse shape hopping scheme for the DS or TH UWB signal format. Simulation results show significant performance improvements by using the proposed UWB system.

key words: *UWB-WPAN, modulated and modified Hermite pulse (MMHP), pulse shape hopping, asynchronous communication, interference reduction*

1. Introduction

Ultra wideband (UWB) communications occupy a very wide transmission bandwidth as its name suggests. More specifically, such a bandwidth has to exceed 500 MHz or 20% of its center frequency. The frequency range is typically in the order of one to several GHz. While UWB communications can achieve high data rate transmission with low complexity, it can provide robustness against various distortions such as multipath fading as well. Hence, UWB wireless communication systems has raised enormous interest in the area of short distance wireless communications [1]. UWB systems have been studied actively since the Federal Communications Commission (FCC) of USA authorized the civil use of UWB signals in February 2002. In such regulation, UWB communication systems have to fullfill a spectral mask that limits the maximum transmission power in order to co-exist with other narrowband and wideband wireless communication systems already operating in the approved spectrum. Indeed, the FCC provides with spectral masks that regulate UWB transmission in the frequency band from 3.1 GHz to 10.6 GHz.

Manuscript received March 3, 2006.
Manuscript revised May 21, 2006.
Final manuscript received July 13, 2006.

[†]The authors are with the Division of Electrical and Computer Engineering, Faculty of Engineering, Yokohama National University, Yokohama-shi, 240-8501 Japan.
a) E-mail: hhiroki@ieee.org
b) E-mail: kohno@ynu.ac.jp

DOI: 10.1093/ietfec/e89–a.11.3050

Originally, UWB communication systems was proposed as impulse radio (IR) UWB, which is based on the transmission of baseband pulses. However, different types of UWB systems based on conventional carrier-based communications have been proposed as well. For instance, multi-band OFDM and DS-UWB systems consider the use of set of carriers and a carrier signal, respectively [2]–[4]. UWB systems that introduce such conventional technologies are effective in terms of feasibility [5]. However, such systems lose some advantages, e.g., low power consumption and simple circuitry.

In multiple access schemes using DS or TH, a pulse position modulation (PPM), a bi-phase modulation and a pulse shape modulation have been proposed [6]–[8]. Additionally, as a transmitting waveform, a monocycle waveform and some orthogonal pulses have also been proposed [9], [10]. Modified Hermite pulses are generated by Hermite polynomials that are modified to become orthogonal [11]. An orthogonal pulse modulation (OPM) is proposed in [12]. The OPM is effective in the case of synchronous communications. However, OPM loses the orthogonality property in the case of asynchronous communications [13].

The performance degradation in terms of bit error probability is mainly caused by three factors [2]. The first is multi-user interference (MUI) from other users in the system. The second is inter-symbol interference (ISI), which is caused by frequency selective channels. The third is co-channel interference such as narrow band interference (NBI), which is the interference from co-existing narrowband and wideband communication systems. For instance, 5 GHz WLAN systems. In UWB-WPAN systems, it is required that the system reduces these interferences effectively.

In this paper, we examine the UWB communication system that uses *modulated and modified Hermite pulses* (MMHP). The MMHP are modulated pulses based on modified Hermite polynomials (MHP). In addition, we design a novel pulse set that occupy the same bandwidth for all orders in order to satisfy the FCC spectral mask effectively. Our proposed MMHP pulse set is denominated as *limited bandwidth MMHP set*. It is composed of pseudo-orthogonal pulses of different order with good correlation characteristics. That is, the cross-correlation values of the proposed MMHP are low, and additionally the spectrum of the MMHP has notches, whose number is the same as the MMHP order. In the proposed system, users use MMHP of different orders at the same time in combination with either

DS or TH so that the effect of MUI can be reduced.

Furthermore, our proposed system can resolve the problem of co-existence between UWB systems and other systems. For instance, the WLAN system "IEEE802.11a," which is allocated around 5 GHz [14]. We use notches of the proposed MMHP to reduce the overlap between the spectrum of the proposed UWB system and the spectrum of the WLAN system so that NBI is reduced effectively.

In the literature [3], [15], [16], several proposals to deal with interferences can be found. However, those solutions introduce more complexity to the system. Alternatively, we develop the novel pulse set as well as the innovative method of pulse shape hopping, which outperforms conventional systems in terms of interference suppression. Additionally, by using the novel pulse set together with pulse shape hopping scheme, the proposed system keeps also the advantage of low transceiver complexity.

The rest of the paper is organized as follows. The conventional DS-UWB and TH-UWB systems are described in Sect. 2. In Sect. 3, we outline our proposed UWB system using the limited bandwidth MMHP set. In Sect. 4, numerical comparison between the proposed system and the conventional UWB system is presented. Finally, conclusions and future work are remarked in Sect. 5.

2. TH-UWB and DS-UWB System Model

In this section we revise briefly the conventional TH-UWB system [1] and DS-UWB system [2], [3]. We consider the TH-UWB system and the DS-UWB system as a benchmark for our proposed system, since TH-UWB and DS-UWB systems have simple circuitry and low power consumption.

Normally, two types of data modulation are considered for TH-UWB systems, binary antipodal modulation and binary PPM. The binary antipodal modulation scheme outperforms binary PPM scheme in terms of bit error probability. Moreover, polarity reversals can eliminate the spectral lines and reduce the peak-to-average ratio. Thus, the binary antipodal modulation scheme is used as a data modulation scheme in our proposed system throughout the paper. However our results can be readily extended to binary PPM.

2.1 TH-UWB System Model

TH-UWB impulse radio is built upon position shift of pulses with a certain shape in the time domain. A system with TH-UWB can accommodate multiple simultaneous users by assigning an appropriate hopping sequence to each user in asynchronous communications. In TH-UWB, the transmitted signal from the k-th transmitter using binary antipodal modulation can be defined as

$$s_t^{(k)}(t) = \sum_{i=0}^{\infty} b^{(k,i)} \sum_{j=0}^{N_s-1} w_{tr}(t - jT_f - c_t^{(k,j)}T_c - iT_b), \quad (1)$$

where $w_{tr}(t)$ is the transmission pulse shape, and $b^{(k,i)} \in \{\pm 1\}$ is a binary information bit sequence for the k-th user. $w_{tr}(t-jT_f-c_t^{(k,j)}T_c-iT_b)$ indicates the j-th pulse transmitted by the k-th user at $t = jT_f + c_t^{(k,j)}T_c + iT_b$. The pseudorandom time-hopping sequence for the k-th user is given by $[c_t^{(k,0)}, c_t^{(k,1)}, \ldots, c_t^{(k,N_s-1)}]^T$, where $c_t^{(k,j)} \in [0, N_h]$. T_c is the chip duration and T_f is the frame duration, which is greater than or equal to N_hT_c. The information bit duration is represented by T_b. The number of hops in each bit duration is designated by N_s, and T_b equals N_s times frame duration T_f, i.e., $T_b = N_sT_f$.

2.2 DS-UWB System Model

DS-UWB system employs transmission pulses that are spreaded by pseudorandom sequences in the chip level. Since different sequences are assigned to users, DS-UWB system can accommodate multiple simultaneous users as well as TH-UWB system. In DS-UWB, the transmitted signal from the k-th transmitter using binary antipodal modulation can be defined as

$$s_d^{(k)}(t) = \sum_{i=0}^{\infty} b^{(k,i)} \sum_{j=0}^{N_s-1} c_d^{(k,j)} \cdot w_{tr}(t - jT_c - iT_b), \quad (2)$$

where the information bit duration is represented by $T_b = N_sT_c$. The pseudorandom spreading sequence for k-th user is given by $[c_d^{(k,0)}, c_d^{(k,1)}, \ldots, c_d^{(k,N_s-1)}]^T$, where $c_d^{(k,j)} \in \{\pm 1\}$. It is known that DS-UWB outperforms TH-UWB when the number of users is lower than the spreading factor N_s [17]. On the contrary, when MUI is dominant, both DS and TH systems exhibit similar performance.

2.3 Received Signal Representation

If there are N_u active users in the system, the composite received signal at the output of the receiver antenna is given by

$$r(t) = \sum_{k=0}^{N_u-1} h^{(k)}(t) \otimes s^{(k)}(t) + \nu(t), \quad (3)$$

where $h^{(k)}(t)$ is the k-th UWB channel impulse responce, $s^{(k)}(t)$ represents the received signal from the k-th transmitter, and $\nu(t)$ represents composite noises that include NBI and the thermal noise. Without loss of generality, we assume that user $k = k'$ is the detection target. Therefore, (3) can be rewritten as

$$r(t) = h^{(k')}(t) \otimes s^{(k')}(t) + \sum_{k \neq k'}^{N_u-1} h^{(k)}(t) \otimes s^{(k)}(t) + \nu_n(t) + \nu_a(t), \quad (4)$$

where $\nu_n(t)$ is NBI and $\nu_a(t)$ is additive white Gaussian noise (AWGN). In (4), the first term represents target signal including ISI. On the other hand, the second term of (3) represents MUI.

UWB channels have a large delay spread. Thus, UWB

communications suffer from ISI severely. We here employ the IEEE802.15.3a channel model as the UWB multipath fading channel model throughout the paper [18].

Originally, IR-UWB systems employing short baseband pulses, those were implemented by exciting a conventional monopole antenna with a stepped in amplitude method, whose output can be modeled mathematically as the first derivative of a gaussian pulse [1]. So, it had been assumed that the transmitted UWB pulse shape is distorted by transmit and receive antennas [19]. However, novel UWB antenna designs do not introduce waveform distortions such as derivative effects [20].

3. Proposed UWB System Using Novel Pulse Set

In this section we explain our proposed UWB system using the MMHP.

3.1 Pulse Set Design (Limited Bandwidth)

A given user sends pulses in a certain timing pattern with an unique DS or TH sequence. In our proposed system, users utilize modified MMHP waveforms of various orders, in contrast to the case of single pulse waveform in conventional DS-UWB and TH-UWB systems. The MMHP and their characteristics are described below.

Hermite polynomials are modified to become orthogonal and are represented as follows [11]

$$g^{(n)}(t) = e^{-\frac{t^2}{4}} h_e^{(n)}(t) = (-1)^n e^{\frac{t^2}{4}} \frac{d^n}{dt^n}\left(e^{-\frac{t^2}{2}}\right), \quad (5)$$

where $h_e^{(n)}(t)$ is Hermite polynomial and n is the order of this MHP. Thus, MHP functions with different order are orthogonal to each other when they are perfectly aligned. However, the FCC spectral mask regulates the use frequencies from 3.1 GHz to 10.6 GHz. Unfortunately, MHP pulses do not fulfill this spectral mask [21]. Thus, the MHP pulses are modulated by a carrier signal of frequency f_c represented as

$$\begin{aligned} g_m^{(n)}(t) &= g^{(n)}(t)\cos(2\pi f_c t) \\ &= (-1)^n \cos(2\pi f_c t) e^{\frac{t^2}{4}} \frac{d^n}{dt^n}\left(e^{-\frac{t^2}{2}}\right). \end{aligned} \quad (6)$$

Equation (6) is denominated as MMHP waveform. Figures 1 and 2 show the time and frequency domain representations of the MMHP for $f_c = 6.85$ GHz, and orders $n = 0, 1, 2, 3, 4$.

The MMHP can fulfill the FCC spectral mask. Additionally, the MMHP are efficient waveforms since the MMHP can be generated by an oscillator and the simple MHP generator [12].

However, the bandwidth of the MMHP extends as the order increases. Therefore, the MMHP of higher order cannot be used in the case of fulfilling the FCC spectral mask [21]. Moreover, different orders of the MMHP have different bandwidth respectively. Since, robustness against multipath fading varies with the order of the transmitted MMHP.

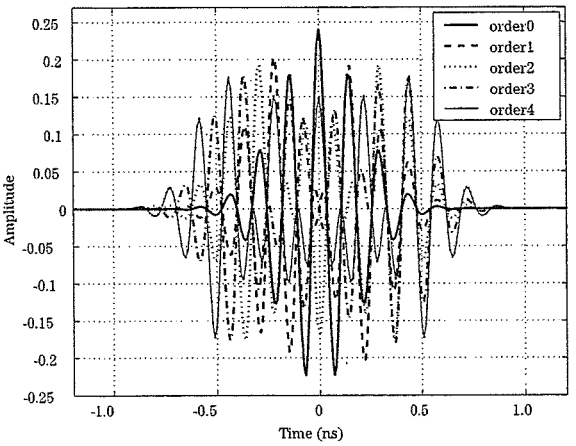

Fig. 1 The time domain representation of the MMHP: order 0, 1, 2, 3, 4.

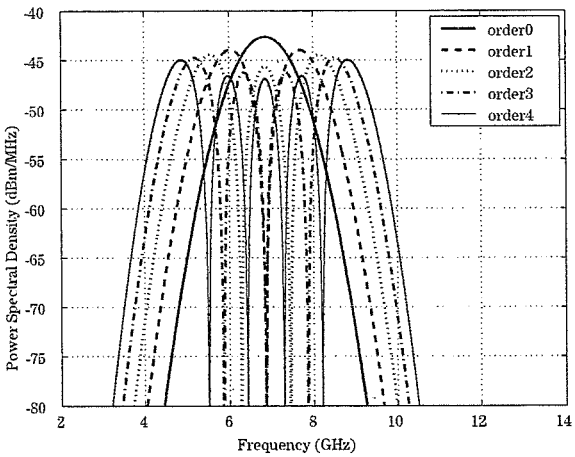

Fig. 2 The frequency domain representation of the MMHP: order 0, 1, 2, 3, 4.

So, we improve the waveforms to resolve these problems. Equation (6) can be transformed as follows

$$\begin{aligned} g_{LB}^{(n)}(t) = N^{(n)}(-1)^n \cos(2\pi f_c t) \exp\left[\frac{\left(\frac{t}{t_p}\right)^2}{4}\right] \\ \cdot \frac{d^n}{dt^n}\left(\exp\left[-\frac{\left(\frac{t}{t_p}\right)^2}{2}\right]\right). \end{aligned} \quad (7)$$

$N^{(n)}$ is a normalizing parameter and t_p is a parameter which controls the pulse width. If t_p increases, the bandwidth of the pulse becomes narrower. Table 1 shows the pulse width and the limit of the enabled orders when the bandwidth fits into the 3.1 GHz to 10.6 GHz band. The value of t_p is fixed properly for each order so that the MMHP of different orders have the same bandwidth. Consequently, even if the MMHP of higher order are used, the bandwidth can be fit into the bounds of the spectral mask as shown in Fig. 3, where the

Table 1 The suitable values of pulse width parameters and the orders for a 3.1 GHz to 10.6 GHz bandwidth.

order n	pulse width parameter t_p (nsec)
0	0.0375
1	0.0625
2	0.0781
3	0.0906
4	0.1031
5	0.1125
6	0.1219
7	0.1313
8	0.1375

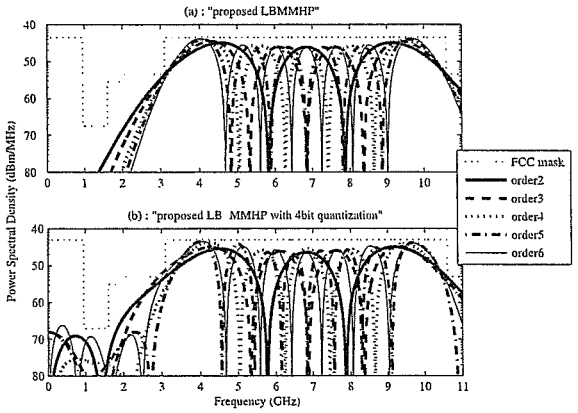

Fig. 3 The frequency domain representation of the limited bandwidth MMHP set: order 2, 3, 4, 5, 6.

sampling frequency is 25 GHz. The proposed pulse set is denominated as *limited bandwidth MMHP (LB-MMHP) set.*

The novel set of LB-MMHP that is generated in this way has the following characteristics:

- LB-MMHP with different order are pseudo-orthogonal to each other when they are perfectly aligned.
- LB-MMHP waveforms have sharp auto-correlation characteristics in all orders in contrast to the conventional set of MMHP waveforms.
- The cross-correlation between different orders is low and independent of the time lag.
- The spectrum of each LB-MMHP of different order has notches whose number is the same as its order.

3.2 Correlation Characteristics Analysis

As follows, we confirm correlation characteristics of the LB-MMHP set.

The correlation value of the proposed LB-MMHP $C^{(m,n)}(\tau)$ is given by

$$C^{(m,n)}(\tau) = \int_{-\infty}^{\infty} g_{LB}^{(m)}(t) \cdot g_{LB}^{(n)}(t-\tau)dt. \quad (8)$$

Table 2 shows the correlation values of the proposed LB-MMHP in the case of $\tau = 0$. This table indicates that the orthogonality is lost when the bandwidth of all orders fits into the spectral mask. However, the correlation values are

Table 2 Correlation values $C_{m,n}(0)$ of the proposed LB-MMHP for a 3.1 GHz to 10.6 GHz bandwidth.

m, n	0	1	2	3	4	5	6	7	8
0	1	0	−0.4	0	0.3	0	−0.2	0	0.2
1	-	1	0	−0.4	0	0.3	0	−0.3	0
2	-	-	1	0	−0.4	0	0.3	0	−0.3
3	-	-	-	1	0	−0.4	0	0.3	0
4	-	-	-	-	1	0	−0.4	0	0.3
5	-	-	-	-	-	1	0	−0.4	0
6	-	-	-	-	-	-	1	0	−0.4
7	-	-	-	-	-	-	-	1	0
8	-	-	-	-	-	-	-	-	1

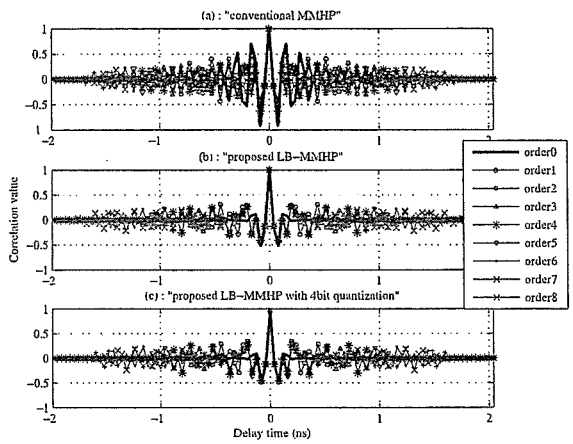

Fig. 4 An auto-correlation characteristic of both conventional MMHP, proposed LB-MMHP and LB-MMHP with 4 bit quantization levels of order ranging from 0 to 8.

zero in the cases of both $m + n = 2i + 1$ $(i = 0, 1, 2, ...)$ and $m \neq n$. Additionally, the correlation values are low in the cases of both $m + n = 2i$ and $m \neq n$. So, we can consider the LB-MMHP as a pseudo-orthogonal pulse set.

Figure 4 shows the auto-correlation characteristic of both the conventional MMHP, the LB-MMHP and the LB-MMHP with 4 bit quantization levels based on Eq. (8). Auto-correlations of proposed LB-MMHP of all orders have the same peaks and low auto-correlation values around time lag 0, as contrasted to the conventional MMHP. This improvement of correlation is caused by changing the pulse durations of MMHP.

On the other hand, Fig. 5 shows the cross-correlation characteristics of both the conventional MMHP, the LB-MMHP and the LB-MMHP with 4 bit quantization levels based on Eq. (8). We can see that the cross-correlation between different orders is lower than the auto-correlation and independent of the time lag in the cases of both conventional MMHP and proposed LB-MMHP.

Furthermore, by Figs. 4 and 5, we can see that the 4 bit quantization levels are enough for proposed pulses to keep their correlation characteristics. Since less than 4 bit quantization levels will cause performance degradation of correlation characteristics, so these waveforms need over 4 bit quantization levels. Additionally, power spectral densities of quantized waveforms are shown as Fig. 3(b). Al-

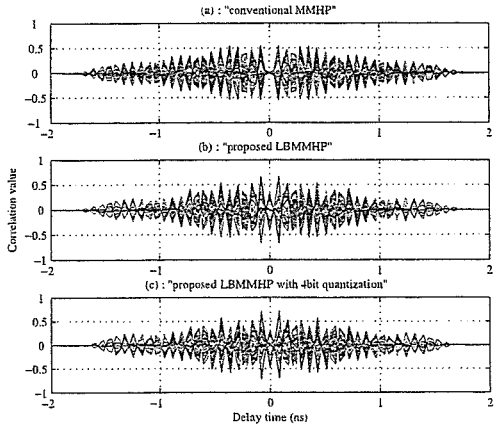

Fig. 5 A cross-correlation characteristic of both conventional MMHP, proposed LB-MMHP and LB-MMHP with 4 bit quantization levels of all combinations of orders ranging from 0 to 8.

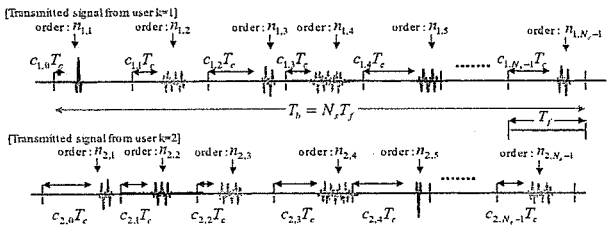

Fig. 6 Transmitted signals from user $k = 1$ and user $k = 2$ in our proposed TH system using the LB-MMHP set and pulse shape hopping.

though they are different from original power spectral densities, they can fulfill FCC indoor spectral mask except for orders 0 and 1.

3.3 Pulse Shape Hopping Using the LB-MMHP Set

As a way of reducing effects of ISI and MUI, we propose the pulse shape hopping using LB-MMHP.

In the proposed scheme with TH, a user employs LB-MMHP of different orders following a time hopping sequence as illustrated in Fig. 6. Thus, a user sends the LB-MMHP waveform whose order is decided by a unique pseudo-random noise (PN) sequence to hop the order, in exact timing with an unique time hopping (TH) sequence. The k-th user's transmitted signal $s_{TH}^{(k)}(t)$ is given by

$$s_{TH}^{(k)}(t) = \sum_{i=0}^{\infty} b^{(k,i)} \sum_{j=0}^{N_s-1} g_{LB}^{(n_{k,i,j})}(t - jT_f - c_t^{(k,j)}T_c - iT_b), \tag{9}$$

where the sequence set elements $n_{k,i,j}$ is a pseudorandom pulse shape hopping sequence for the k-th user, whose range is between the minimum hopping order of the LB-MMHP n_{min} and the maximum hopping order of the LB-MMHP n_{max}.

Additionally, the proposed scheme can be also applied to DS-UWB systems as well. In the proposed scheme with

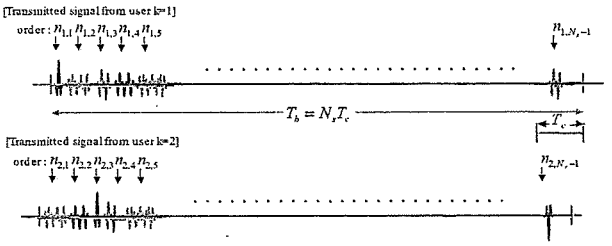

Fig. 7 Transmitted signals from user $k = 1$ and user $k = 2$ in our proposed DS system using the LB-MMHP set and pulse shape hopping.

DS, the k-th user's transmitted signal $s_{DS}^{(k)}(t)$ is given by

$$s_{DS}^{(k)}(t) = \sum_{i=0}^{\infty} b^{(k,i)} \sum_{j=0}^{N_s-1} c_d^{(k,j)} \cdot g_{LB}^{(n_{k,i,j})}(t - jT_c - iT_b), \tag{10}$$

as illustrated in Fig. 7.

We assume that the receiver has knowledge of both the time-hopping sequence and the pulse shape hopping sequence of the desired user. Additionally, perfect synchronization is assumed. A correlator in the receiver measures the correlation values between the received signal $r(t)$ and a template signal $v(t)$. Data are demodulated by the correlation detection. This operation is represented by

$$CP^{(k,i)} = \int_{iT_b}^{(i+1)T_b} r(t) \cdot v^{(k)}(t - iT_b)dt, \tag{11}$$

$$\hat{b}^{(k,i)} = sgn(CP^{(k,i)}), \tag{12}$$

where CP is the output of the correlator, $\hat{b}^{(k,i)}$ is the decision statistic of the coherent detection, and the template signal $v(t)$ is given by

$$v^{(k)}(t) = \begin{cases} \sum_{j=0}^{N_s-1} c_d^{(k,j)} \cdot g_{LB}^{(n_{k,i,j})}(t - jT_c) \\ \text{for DS,} \\ \sum_{j=0}^{N_s-1} g_{LB}^{(n_{k,i,j})}(t - jT_f - c_t^{(k,j)}T_c) \\ \text{for TH.} \end{cases} \tag{13}$$

The received signal $r(t)$ includes not only the desired signal $s^{(k)}(t)$, but also the interference signal from other users, ISI, and all other kinds of noise sources.

As it is described in Sect. 1, the ISI is caused by the effect of multi-path fading. Delayed pulses of a signal interfere with next pulses in particular the case of a high data rate communication. The level of ISI is decided by the channel's delay spread and the auto-correlation function of the transmitted signal.

For asynchronous communication, the correlation output of the MUI component is given by

$$MUI = \int_0^{N_s \cdot T_f} \left[\sum_{k \neq k'}^{N_u} h^{(k)}(t) \otimes s^{(k)}(t - \tau_k) \right] \cdot v(t)dt, \tag{14}$$

where $s^{(k)}(t)$ is the transmitted signal of k-th user, τ_k is a random delay time, and N_u is the number of users in the system. The value of MUI is decided by the cross-correlation function between other user's signals $k \neq k'$ and the template signal for desired user k'.

Therefore, MUI can be reduced if users use different pulses that have low cross-correlation characteristics each other simultaneously. The cross-correlation between the proposed LB-MMHP of different orders is low and independent of the time lag as it is described in Sect. 3.2. So, the proposed system employs a Reed-Solomon (RS) sequences as the pulse shape hopping sequences for users in order to keep the number of waveforms as few as possible. For instance, a RS sequence is used to select the MMHP that forms a user signature waveform, such that a given MMHP is just repeated 1 time for another user's signature waveform at the same chip time.

The MMHP generator of our proposed system needs a MHP generator and only one oscillator. Additionally, the MHP of higher order is generated by the MHP of low order and derivative circuits [11], [12]. However, generating the proposed pulses by analog circuitry requires high-precision devices such as delay lines that can make a long delay, high-precision variable attenuator, and so on. So, it is difficult for current technologies to generate such complex waveforms by analog circuitry. On the other hand, LB-MMHP can be synthesized with digital technology relatively easy. Although it requires very fast digital to analog converters (DACs), the advances on high speed electronics will make available the required DACs with a reasonable cost. Additionally, Figs. 4 and 5 indicate that a DAC with 4 bit quantization might be enough for our proposed pulses to maintain correlation characteristics. Since pulses occupy the frequency band from 3.1 GHz to 10.6 GHz, the DAC should have over 15 GHz sampling frequency. Because such DAC increases the cost significantly, alternatively, there is a scheme which can reduce the cost by using several parallel DAC of low sampling frequency instead of the DAC with high sampling frequency [22]. Consequently, we consider that it is possible to generate our proposed pulses with reasonable cost and high-precision. As compared with conventional UWB systems for WPAN, our system does not have complex circuitry including FFT such as multiband OFDM, and requires shorter spreading sequences for multiple access than spreading sequences of DS-UWB. So also in terms of hardware feasibility, our proposed system can countervail conventional systems.

4. Performance Evaluation

In this section we describe the result of performance evaluation.

4.1 Simulation Model

We consider the indoor short-distance multipath fading channel as the UWB communication environment and use the IEEE802.15.3a channel model [18]. Additionally, since DS-UWB is more practical than TH-UWB for WPAN, we use the conventional DS-UWB system and the proposed system combined with DS in our simulations.

Table 3 Parameters of the simulations.

channel model	CM1,2,3,4
number of transmitted bits	10^5
bandwidth	3.1–10.6 (GHz)
used LB-MMHP order	2–9
number of users	1,4,8,16
data modulation	bi-phase modulation
chip duration	2.6 (nsec)
time duration of 1 bit	2.6–49.4 (nsec)
number of pulse repetitions N_s	1–19
datarate	20.2–384.6 (Mbps)
receiver	Selective RAKE
number of fingers	1–50
combining	MRC
E_b/N_0	0–18 (dB)
SIR	−20–−4 (dB)

We assume an asynchronous communication system. In order to make simulations simple, the following assumptions are made:

- The transmitting pulses are quantized by 4 bit quantization levels, and there are no quantization in the receiver.
- The desired signal and the template signal are perfectly synchronized.
- Simulations do not include error correcting codes.
- The receiver knows both the DS sequence and the pulse shape hopping sequence used by the desired user.
- A Gold sequence is applied as the DS sequence in both our proposed system and a conventional DS-UWB system.
- A RS sequence is applied as the pulse shape hopping sequence in our proposed system.
- Signal to Interference Ratio (SIR) is defined as

$$SIR = \frac{\int_0^{T_b} |s^{(k)}(t)|^2 dt}{\sum_{k' \neq k}^{N_u} \int_0^{T_b} |s^{(k')}(t)|^2 dt}. \quad (15)$$

We use the 6-th derivative of Gaussian pulse in the conventional DS-UWB system for comparison. The bandwidth of this pulse can fulfill the FCC spectral mask. Parameters of the simulations are shown in Table 3.

4.2 Results

Figure 8 illustrates the BER performance for CM1 channels with $N_u = 1, 4, 8, 16$ users. In this figure, the proposed UWB system with DS as shown by Eq. (10) are compared to the conventional DS-UWB system using the 6-th derivative of a Gaussian pulse. Notice that our proposal offers better performance than the BER performance of the conventional system, specially in the case of multiple access. So, the pulse shape hopping scheme using LB-MMHP waveforms can reduce the effects of MUI and ISI since our proposal offers transmitted signals that have both good auto-

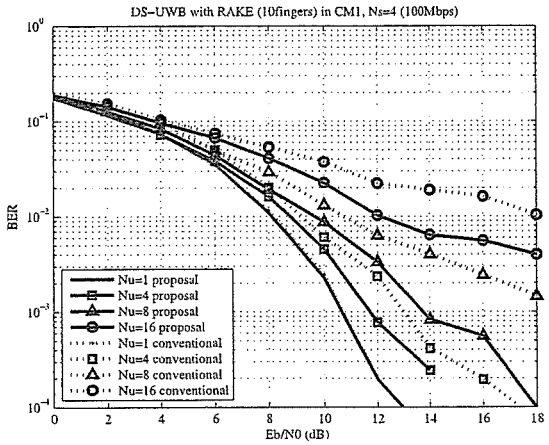

Fig. 8 BER performance of the proposed system with DS and the conventional DS-UWB system in CM1.

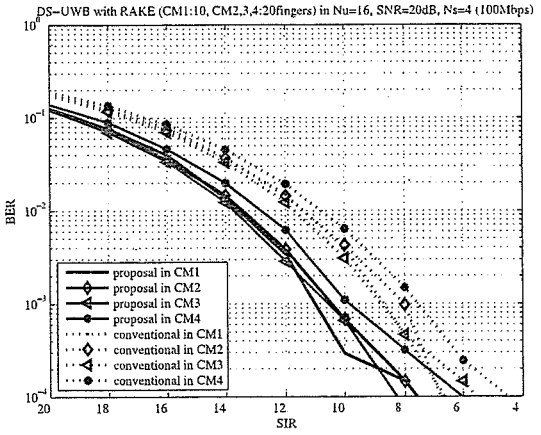

Fig. 10 SIR versus BER performance of the proposed system with DS and the conventional DS-UWB system in CM1,2,3 and 4.

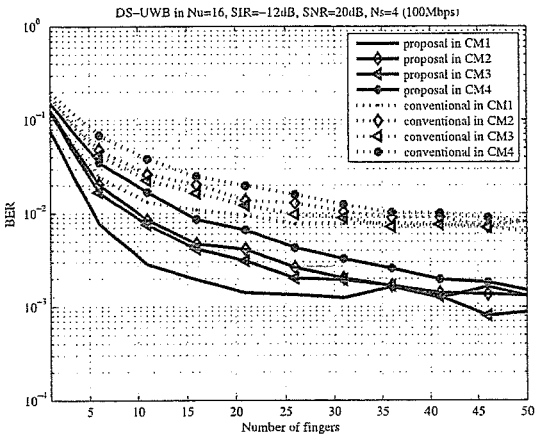

Fig. 9 Different number of RAKE fingers versus BER performance of the proposed system with DS and the conventional DS-UWB system in CM1,2,3 and 4.

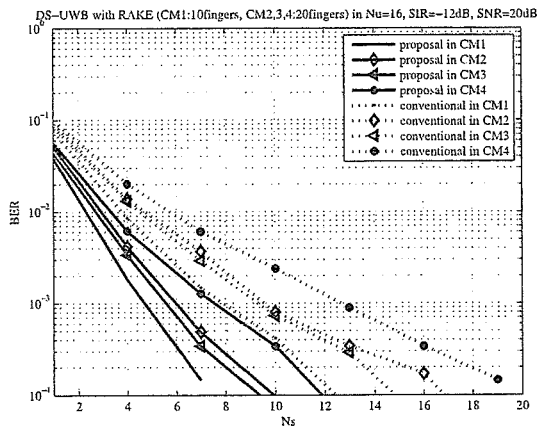

Fig. 11 N_s versus BER performance of the proposed system with DS and the conventional DS-UWB system in CM1,2,3 and 4.

correlation and low cross-correlation properties by employing LB-MMHP waveforms.

Figure 9 indicates the impact in performance of different number of RAKE fingers. We can see that around 10 fingers bring a modest performance in CM1, and around 20 fingers in CM2, 3 and 4. Additionally, the conventional system can not outperform our proposal even if the conventional system uses a large number of fingers in the RAKE receiver.

Figure 10 shows the impact in performance of different SIR levels. The gain of our proposal is around 2 dB in terms of SIR, and is independent from SIR level. So, our proposal outperforms the conventional system under both high SIR and low SIR situations.

Figure 11 shows the impact in performance of the processing gain N_s. As the processing gain N_s increases, the data information rate decreases. We can see that the proposed system offers good performance for both the high data rate and low data rate cases.

4.3 Effect of Proposed Scheme for Reducing NBI (Coexistence between UWB System and Other Systems)

UWB communication systems need to coexist with other systems [14]. For example, UWB-WPAN systems that occupy the frequency band from 3.1 GHz to 10.6 GHz might be interfered by WLAN systems in the 5 GHz-band.

Nevertheless, we can adopt proper countermeasures against this problem. The spectrum of the LB-MMHP has some notches (see Fig. 3). If a notch is placed in the 5 GHz-band, NBI can be reduced. Therefore, our proposed system uses only LB-MMHP of suitable orders, in the case of co-existence. Figure 12 shows the power spectral density of LB-MMHP with suitable orders, such that notches are formed in the 5 GHz band of WLAN systems.

Figure 13 shows the characteristics of the bit error rates of the proposed system and the conventional DS-UWB system when we vary from the desired to the undesired ratio (DUR) by changing from 0 dB to −30 dB. DUR is given by

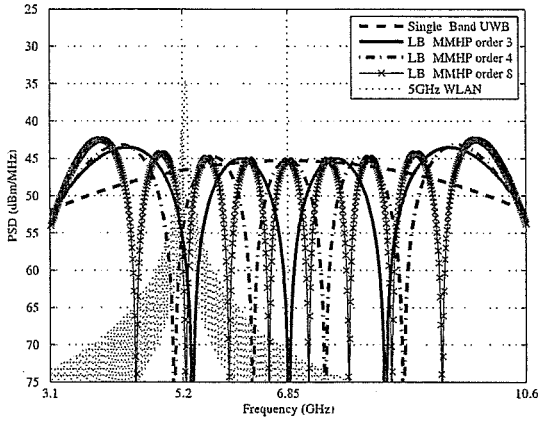

Fig. 12 The power spectral density of the LB-MMHP of order 3, 4 and 8, the single-band pulse and WLAN system (5 GHz-band, $DUR = 0$ dB).

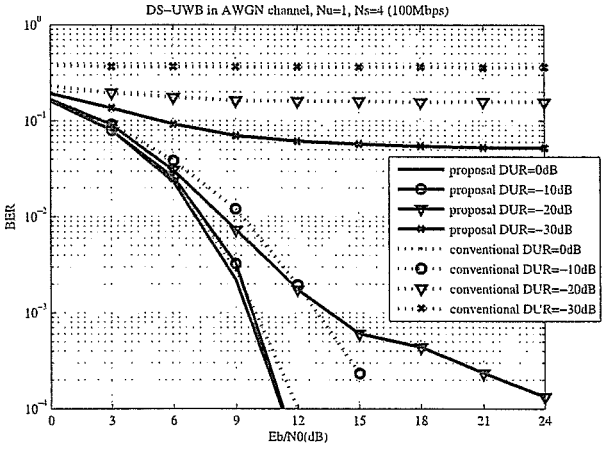

Fig. 13 The bit error rate of the proposed system and the conventional DS-UWB system in the case of co-existence with 5 GHz WLAN system in AWGN channel.

$$DUR = \frac{\int_0^{T_b} |s^{(k)}(t)|^2 dt}{\int_0^{T_b} |\nu_n(t)|^2 dt}, \tag{16}$$

where $\nu_n(t)$ is a narrow band interference signal, and we apply OFDM signals implemented in IEEE802.11a as $\nu_n(t)$ in our simulations. Additionally, T_b is the duration of UWB signal for 1 bit. We can see that the proposed system outperforms the conventional DS-UWB system in terms of the bit error rate, especially in the case of $DUR = -10, -20$ dB.

5. Conclusions

We proposed the UWB communication system for reducing various interferences. We designed a novel pulse set called *LB-MMHP set* to comply with the FCC spectral mask. We confirmed that our proposed system outperforms the conventional DS-UWB systems in terms of the bit error rate. Our proposed pulse shape hopping scheme can reduce effects of MUI and ISI effectively. Additionally, the problem of co-existence between UWB systems and WLAN systems is solved by using notches of the proposed LB-MMHP.

The performance evaluation with other waveforms, and the effect of timing jitter, will be studied as future research.

References

[1] M.Z. Win and R.A. Scholtz, "Ultra-wide bandwidth time-hopping spread-spectrum impulse radio for wireless multiple-access communications," IEEE Trans. Commun., vol.48, no.4, pp.679–691, April 2000.

[2] J. Foerster, "The performance of a direct-sequence spread ultra-wideband system in the presence of multipath, narrowband interference and multiuser interference," Proc. IEEE Conf. Ultra Wideband Systems and Technologies, Digest of Papers, pp.87–91, Baltimore, MD, May 2002.

[3] Q. Li and L.A. Rusch, "Multiuser detection for DS-CDMA UWB in the home environment," IEEE J. Sel. Areas Commun., vol.20, no.9, pp.1701–1711, Dec. 2002.

[4] J. Foerster, V. Somayazulu, S. Roy, E. Green, K. Tinsley, C. Brabenac, D. Leeper, M. Ho, and Intel, "Intel's multi-band UWB PHY proposal for IEEE 802.15.3a," IEEE P802.15 Wireless Personal Area Networks, P802.15-03/109r1, March 2003.

[5] G. Durisi, J. Romme, and S. Benedetto, "Performance of TH and DS UWB multiaccess systems in presence of multipath channel and narrowband interference," Proc. IWUWBS 2003, Oulu, Finland, June 2003.

[6] R.A. Scholtz, "Multiple access with time hopping impulse modulation," Proc. Military Communications Conference (MILCOM'93), pp.447–450, Boston, MA, Oct. 1993.

[7] G. Durisi and G. Romano, "On the validity of gaussian approximation to characterize the multiuser capacity of UWB TH-PPM," Proc. IEEE Conf. Ultra Wideband Systems and Technologies, Digest of Papers, pp.157–161, Baltimore, MD, May 2002.

[8] M. Ghavami, L.B. Michael, S. Haruyama, and R. Kohno, "A novel UWB pulse shape modulation system," Wirel. Pers. Commun., vol.23, no.1, pp.105–120, Oct. 2002.

[9] X. Wu, Z. Tian, T.N. Davidson, and G.B. Giannakis, "Optimal waveform design for UWB radios," Proc. ICASSP 2004, pp.521–524, Quebec, Canada, May 2004.

[10] G.T.F. de Abreu, C.J. Mitchell, and R. Kohno, "On the orthogonality of hermite pulses for ultra wideband communications systems," Proc. Wireless Personal Multimedia Conf. (WPMC'03), pp.288–292, Yokosuka, Japan, Oct. 2003.

[11] M. Ghavami, L. Michael, and R. Kohno, Ultra Wideband Signals and Systems in Communication Engineering, John Wiley & Sons, 2004.

[12] L.B. Michael, M. Ghavami, and R. Kohno, "Multiple pulse generator for ultra-wideband communication using hermite polynomial based orthogonal pulses," Proc. IEEE Conf. Ultra Wideband Systems and Technologies, Digest of Papers, pp.47–51, Baltimore, MD, May 2002.

[13] H. Harada, T. Sato, and R. Kohno, "Multivalued transmission system for UWB-CDMA using modified hermite pulse shape," Proc. IEEE Topical Conf. Wireless Communication Technology, pp.451–452, Honolulu, HI, Oct. 2003.

[14] X. Chu and R.D. Murch, "The effect of NBI on UWB time-hopping systems," IEEE Trans. Wirel. Commun., vol.3, no.5, pp.1431–1436, Sept. 2004.

[15] X. Luo, L. Yang, and G.B. Giannakis, "Designing optimal pulse-shapers for ultra-wideband radios," J. Commun. Netw., vol.5, no.4, pp.344–353, Dec. 2003.

[16] J.D. Choi and W.E. Stark, "Performance of ultra-wideband communications with suboptimal receivers in multipath channels," J. Commun. Netw., vol.20, no.9, pp.1754–1766, Dec. 2002.

[17] G. Durisi, A. Tarable, J. Romme, and S. Benedetto, "A general method for error probability computation of uwb systems for in-

door multiuser communications," J. Commun. Netw., vol.5, no.4, pp.354–364, Dec. 2003.

[18] J. Foerster, Q. Li, and Intel, "Channel modeling sub-comitee report final," IEEE P802.15 WG for WPANs Technical Report, P802.15-02/490r1-SG3a, Feb. 2003.

[19] A. Shlivinski, E. Heyman, and R. Kastner, "Antenna characterization in the time domain," IEEE Trans. Antennas Propag., vol.45, no.7, pp.1140–1149, July 1997.

[20] M. Hernandez and R. Kohno, "Signal design for high data rate DS-UWB transmissions in MIMO channels," Proc. IEEE International Conf. on Wireless Networks, Communications, and Mobile Computing, pp.1214–1219, Maui, Hawaii, USA, 2005.

[21] H. Harada, K. Ikemoto, and R. Kohno, "Modulatation and hopping using modified hermite pulses for UWB communications," Proc. IEEE International Workshop on UWB Systems Joint with Conf. UWB Systems and Technologies, pp.336–340, Kyoto, Japan, May 2004.

[22] G. Ono, T. Nakagawa, A. Maeki, R. Fujiwara, T. Norimatsu, K. Mizugaki, M. Miyazaki, M. Kokubo, Y. Okuma, M. Hayakawa, S. Kobayashi, N. Koshizuka, and K. Sakamura, "3-nw/bps low power UWB system (3): Development of RF front end," Symposium of the IEICE Society of Communications, p.134, Sapporo, Japan, Sept. 2005.

Hiroki Harada received the M.E. degree in electrical and computer engineering from Yokohama National University, Yokohama, Japan, in 2005. He is currently working toward the Ph.D. degree in electrical and computer engineering at Yokohama National University, Yokohama, Japan. He is also Research Fellow of the Japan Society for the Promotion of Science. His research interests lie in the area of ultra wideband communication and information theory. He is a student member of IEEE. He is JSPS Research Fellow.

Ryuji Kohno received the Ph.D. degree from the University of Tokyo in 1984. Dr. Kohno is currently a Professor of the Division of Physics, Electrical and Computer Engineering, and the Director of Center on Medical Information and Communication Technology, in Yokohama National University. In his currier he was a director of Advanced Telecommunications Laboratory of SONY CSL during 1998–2002 and currently a director of UWB Technology institute of National Institute of Information and Communications Technology (NICT). In his academic activities, he was elected as a member of the Board of Governors of IEEE Information Theory (IT) Society in 2000 and 2003. He has played a role of an editor of the IEEE Transactions on IT, Communications, and Intelligent Transport Systems (ITS). He has been vice-president of Engineering Sciences Society of IEICE, the Chairman of the IEICE Technical Committee on Spread Spectrum Technology, that on ITS, and that on Software Defined Radio (SDR). Prof. Kohno has contributed for organizing many international conferences, such as an chair-in honor of 2002 & 2003 International Conference of SDR (SDR'02 & SDR'03), a TPC co-chair of 2003 International Workshop on UWB Systems (IWUWBS'03), and a general co-chair of 2003 IEEE International Symposium on IT (ISIT'03), UWBST&IWUWB'04, IWUWBST'05 and so on. He was awarded IEICE Greatest Contribution Award and NTT DoCoMo Mobile Science Award in 1999 and 2002, respectively.

TDOA型センサネットワークにおける階層型粒子フィルタを用いた位置推定法

谷口健太郎[†a)]　　河野　隆二[†b)]

Positioning Algorithm Based on TDOA Measurements Using Layered Particle Filter in Sensor Network

Kentaro TANIGUCHI[†a)] and Ryuji KOHNO[†b)]

あらまし　センサネットワークにおいて，個々のセンサタグの位置情報を正確に把握することは非常に重要である．センサタグの測位方式としては，信号の受信時刻差（Time Difference of Arrival：TDOA）を利用した測位システムが知られているが，従来の線形探索アルゴリズムではマルチパスフェージングや見通し外伝搬路の影響で大幅に測位精度が劣化してしまう．本論文では，このような劣悪な伝搬環境においても信頼性の高い測位を実現する方式として，階層型粒子フィルタを用いた測位アルゴリズムを提案する．提案方式では，複数の基地局ノードが測位対象であるセンサタグからの信号を受信し，二階層にわたって粒子フィルタによる状態量推定を実行する．第一階層では，基地局ノードで得られた個々のTDOA観測値に対し，粒子フィルタを用いてマルチパス補償を行う．この際，非ガウス状態空間モデルを利用することにより，見通し外伝搬路に起因する測定異常値を効果的に除去することが可能となる．続いて第二階層では，修正された全TDOA観測値を用いて，粒子フィルタによる位置推定を行う．第一階層での観測値補正により，最終的に得られる測位精度が大幅に改善されることを示す．また計算機シミュレーションにより，提案アルゴリズムが従来方式に比べてより高精度で，見通し外環境に対してもロバストな測位を実現できることを示す．

キーワード　位置検出，トラッキング，TDOA，粒子フィルタ，センサネットワーク

1. まえがき

無線センサネットワークは，近未来のユビキタス社会を形成するコアテクノロジーとして盛んに研究が進められている[1]．無線センサネットワークにおいて，個々のセンサタグの正確な位置を知ることは非常に重要である．位置情報のないセンシングデータは意味をなさない[2],[3]．

測位技術として広く普及したものにGPS（Global Positioning System）システムが挙げられるが，GPSは微弱な電波を利用するため，屋内や都心の密集エリアでは十分な測位精度を得ることが難しい．このような劣悪な環境でも有効に機能し，GPSに依存しない汎用性の高い測位技術への要求が高まっている．

また，センサネットワークでは個々のセンサタグはできるだけ簡易なハードウェア構成が望まれる．したがって，測位に要する信号処理はインフラ側で実行されることが好ましい．信号の受信時刻差（Time Difference of Arrival：TDOA）を利用する測位方式は，このようなニーズを満たす技術として大きな注目を浴びている[4]～[6]．TDOAに基づく測位では，複数の基地局ノードで観測された信号の受信時刻の差を利用して測位を行う．測位に際して，タグでの送信時刻情報を必要とせず，時刻同期は基地局ノード同士のみに要求される．したがって，移動体であるセンサタグは簡易性・独立性・低消費電力性といった特徴を有することができる．このような観点からTDOAに基づく測位は，センサネットワークに適した方式といえる．

本論文では，室内を移動するタグからの信号を，あらかじめ位置の分かっている複数の基地局ノードで受信し，測位を行うシステムを想定する．基地局ノード

† 横浜国立大学大学院工学府，横浜市
Graduate School of Engineering, Yokohama National University, 79–5 Tokiwadai, Hodogaya, Yokohama-shi, 240–8501 Japan
a) E-mail: kentarou@kohnolab.dnj.ynu.ac.jp
b) E-mail: kohno@ynu.ac.jp

は，得られた受信時刻情報を外部基地局，若しくはマスタノードに送信し，そこでタグの測位やトラッキングを実行する．

TDOA を利用した測位は，マルチパスフェージングや見通し外（Non-Line-of-Sight：NLOS）伝搬によって大幅に精度が劣化してしまうことが知られている．このような位置検出は，不確かな時刻情報に基づく非線形問題となる．従来からあるニュートン法などの線形探索アルゴリズムは，TDOA 観測値に含まれる測定誤差によって大きな影響を受けてしまう [10]．

仮に正確な伝搬路情報が得られるのであれば，これらの見通し外伝搬に起因する測定誤差を補償することが可能である [6]．しかしながら，一般に伝搬路情報を正確に得ることは難しく，伝搬路の推定も容易ではない．

マルチパスや NLOS 伝搬に起因する問題への対策として，本論文では粒子フィルタを利用した新しい測位アルゴリズムを提案する [7], [8]．粒子フィルタは一般にモンテカルロフィルタとしても知られ，非線形状態モデルに対する状態量推定アルゴリズムの一つである [11]．TDOA 型システムを含め，様々な測位・測距アプリケーションへの粒子フィルタの適用が検討されているが，マルチパスや NLOS 伝搬への対策は十分になされていない [5], [12]．粒子フィルタによって伝搬遅延を推定する方式も知られているが，タグと基地局間の時刻同期がとれていなければならず，TDOA 型の測位システムへの適用は難しい [14]．

TDOA 型測位システムにおける NLOS 伝搬の影響を軽減するため，本論文では，階層型粒子フィルタを提案する．提案方式では，二階層の粒子フィルタを用いてタグの位置検出を行う．第一階層では，基地局ノードで観測された TDOA 値のそれぞれに対して，粒子フィルタによるマルチパス補償を行う．個々の観測値には，NLOS 伝搬に起因する測定誤差が含まれるため，粒子フィルタによる状態量推定によって，真の TDOA 値への補正を行う．第一階層での状態量推定に際しては，非ガウシアンの状態空間モデルを用いる．裾の重い非ガウス分布を観測ノイズとしてモデル化することで，高い確率で現れる小さいノイズと，低い確率で現れる大きな観測誤差の両方を表現することが可能となる [16]．このような 2 種類のノイズは，実際の観測値に含まれる AWGN（Additive White Gaussian Noise）成分と，NLOS 伝搬に起因して現れる異常値とに対応づけることができる．従来あるカルマンフィルタでは，このような非線形かつ非ガウスモデルへの状態量推定は不可能であった．提案方式では，一つひとつの TDOA 観測値に対して，粒子フィルタによる推定を行うことで，推定する状態量ベクトルの次元を増やすことなく，効果的に異常値を除去することが可能となる．

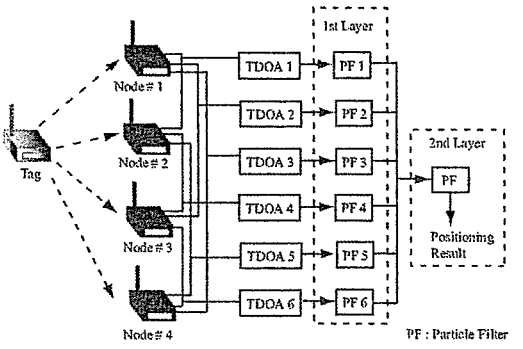

図 1　階層型粒子フィルタを用いた測位システム
Fig. 1　Positioning system using layered particle filter.

第二階層では，第一階層を通して修正されたすべての TDOA 情報を利用して，センサタグの位置推定を行う．この階層ではタグの座標を状態量としてとらえ，粒子フィルタによる状態量推定を行う．提案する測位システムの概要を図 1 に示す．従来からある粒子フィルタによる測位システムは，第一階層を省いて第二階層のみで測位を行うアルゴリズムといえる．この場合，複数得られた TDOA 観測値のうち，大きな誤差を含む観測値の影響を強く受けてしまい，効果的な測位精度を得ることができない．提案方式では，第一階層でのマルチパス補償によって，第二階層での測位精度が大幅に改善され，最終的に理論的下限に近い精度を実現することが可能となる．

本論文では，TDOA 型測位システムについて，実環境に即した伝搬モデルを検討する．劣悪な環境下でも，信頼性の高い測位を実現する階層型粒子フィルタを提案し，その設計・解析を行う．以下，**2.** では想定する測位システムモデルについて述べる．**3.** では提案する階層型粒子フィルタのアルゴリズムを詳細に述べる．**4.** では計算機シミュレーション及び理論解析を通して，提案システムがロバストで高精度な測位を実現できることを示す．

2.　測位システムモデル

2.1　TDOA に基づく測位

本節では，TDOA に基づく測位方式の概要を述べ